The Astrophysical Journal, 651:553–565, 2006 November 1

THE EFFECT OF THE ELECTRIC FIELD INDUCED BY PRECIPITATING ELECTRON BEAMS ON HARD X-RAY PHOTON AND MEAN ELECTRON SPECTRA

Valentina V. Zharkova and Mykola Gordovskyy
Department of Cybernetics and Virtual Systems, University of Bradford, Bradford BD7 1DP, UK;
v.v.zharkova@brad.ac.uk, m.gordovskyy@brad.ac.uk
Received 2005 July 6; accepted 2006 June 1

ABSTRACT

The effect of a self-induced electric field is investigated analytically and numerically on differential and mean electron spectra produced by beam electrons during their precipitation into a flaring atmosphere as well as on the emitted hard X-ray (HXR) photon spectra. The induced electric field is found to be a constant in upper atmospheric layers and to fall sharply in the deeper atmosphere from some "turning point" occurring either in the corona (for intense and softer beams) or in the chromosphere (for weaker and harder beams). The stronger and softer the beam, the higher the electric field before the turning point and the steeper its decrease after it. Analytical solutions are presented for the electric fields, which are constant or decreasing with depth, and the characteristic "electric" stopping depths are compared with the "collisional" ones. A constant electric field is found to decelerate precipitating electrons and to significantly reduce their number in the upper atmospheric depth, resulting in their differential spectra flattening at lower energies ($<$100 keV). While a decreasing electric field slows down the electron deceleration, allowing them to precipitate into deeper atmospheric layers than for a constant electric field, the joint effect of electric and collisional energy losses increases the energy losses by lower energy electrons compared to pure collisions and results in maxima at energies of 40–80 keV in the differential electron spectra. This, in turn, leads to the maxima in the mean source electron spectra and to the "double power law" HXR photon spectra (with flattening at lower energies) similar to those reported from the *RHESSI* observations. The more intense and soft the beams are, the stronger is the lower energy flattening and the higher is the "break" energy where the flattening occurs.

Subject headings: Sun: flares — Sun: particle emission — Sun: X-rays, gamma rays

1. INTRODUCTION

One of the most important effects revealed in many flares from high-resolution *RHESSI* observations are the elbow-type hard X-ray photon spectra with "double power-law" energy distributions (Kontar et al. 2002; Holman et al. 2003; Conway et al. 2003) that cannot be fully interpreted by pure Coulomb collisions. The spectral indices of lower energies ($<$70 keV) are found to be smaller by 1.5–2.5 than those at higher energies. The "break" energy separating these spectral parts varies in the range 30–60 keV, being lower for harder beams and higher for softer ones. Moreover, during the impulsive phase of the same flare the spectral indices of hard X-ray (HXR) photon energy spectra above 35 keV show as soft-hard-soft variations (Lin et al. 2003), and the hardest occurring near the maximum HXR emission (Grigis & Benz 2005).

The inversion of high-resolution photon spectra also revealed that the source mean electron spectra have noticeable dips in the energy range of 20–40 keV (see, e.g., Piana et al. 2003), followed by maxima at higher energies (up to 50–80 keV) where the HXR photon spectra have noticeable flattening. This indicates that the lower energy electrons lose their energy in some processes additional to Coulomb collisions. Although some part of the dips can be explained by HXR albedo from the photosphere (Massone et al. 2004), for the comprehensive interpretation of observed elbow-type photon spectra and inferred mean electron spectra, some additional mechanisms of electron energy losses must be considered.

So far attempts to explain elbow-type photon spectra were focused on a nonuniform ionization of the "thick" target (e.g., Kontar et al. 2003, and references therein) and on a shift of the lower energy cutoff toward higher energies (Holman 2003). However, the variations of ionization do not significantly affect the HXR emission emitted from the corona or chromosphere where the plasma is fully ionized anyway. Also the increase of lower energy cutoffs in the initial beam electron spectra assumed in other studies (Holman 2003) requires some specific mechanisms reducing the production of lower energy electrons ($<$30. . .60 keV) in solar flares that is not anticipated by any acceleration mechanisms, stochastic or by the direct electric field in a reconnecting current sheet.

Thus, this additional mechanism of energy loss by high-energy electrons can be related to the precipitating electrons themselves, i.e., to their energy losses in the electric field induced by them during precipitation into the flaring atmosphere and associated Ohmic heating of the ambient electrons (Knight & Sturrock 1977; Emslie 1980; Diakonov & Somov 1988; Haydock et al. 2001). Steady injection of high-energy ("hot") Maxwellian electrons with kinetic temperatures up to 10^8 K into the cold chromospheric plasma with temperatures of about 10^4 K creates a charged, or turbulent, front separating the "hot" electrons from the ambient plasma (Knight & Sturrock 1977; Brown et al. 1979), which, in turn, leads to the return current formed by the ambient plasma electrons and Ohmic heating of the ambient plasma. This heating is mainly caused by higher energy ($3.92E_0$) beam electrons escaping through this front into the flaring atmosphere (Diakonov & Somov 1988), where E_0 is the average beam energy, or its lower cutoff energy. Assuming that the timescale and length of this front existence coincides with the time and depth of the hot electron precipitation, the Ohmic heating can lead to a significant increase of hard X-ray emission at higher energies and to a change of its polarization sign (Diakonov & Somov 1988).

However, for nonthermal electron beams with power-law energy distributions the effect of a self-induced electric field was

investigated by neglecting the plasma turbulence (Emslie 1980) since it occurs only in a very thin layer just below the injection point (Brown et al. 1979). By solving the energy and momentum conservation equations for a precipitating beam including both collisional and Ohmic energy losses, the induced electric field was also shown to significantly increase compared to pure collisions of the energy deposited in the upper part of a flaring atmosphere that results in the substantial hard X-ray emission and even its saturation for the beams with high initial fluxes (Emslie 1980).

The above approach of neglecting the ambient plasma heating by higher energy electrons escaping through the turbulent front assumed by Diakonov & Somov (1988) was supported by hydrodynamic simulations (Somov et al. 1981, 1982; Nagai & Emslie 1984). The flaring atmospheres are found to respond to the injection of high-energy electron beams or thermal fluxes with fast (a few milliseconds) hydrodynamic heating of the upper atmosphere to high coronal temperatures of 10^6 K (Somov et al. 1981, 1982; Nagai & Emslie 1984). As a result of this response, within 0.1 s a thermoconductive front is formed that moves upward with a speed of about 10^3 km s^{-1}, which is much higher than the speed of ion-acoustic waves produced by the turbulent front (100 km s^{-1}; Somov et al. 1982). As a result, the turbulent front separating the hot electrons and cold plasma is likely to be very quickly (under 1 s) destroyed by the thermoconductive front that is valid for the injection of both thermal (Somov et al. 1982) and nonthermal electrons (Somov et al. 1981; Fisher et al. 1984; Nagai & Emslie 1984).

This allows us to exclude the plasma turbulence from the kinetic approach and to concentrate only on the interaction of beam electrons with the ambient particles. This approach has been implemented by using the time-dependent Fokker-Plank equation for beam electrons precipitating into a flaring atmosphere with exponential variations of density and temperature and taking into account both collisions with the ambient particles and Ohmic losses (McClements 1992; Zharkova et al. 1995). Some precipitating electrons with lower energies ($\leq$100 keV) are found to lose much more energy in the electric field and to be scattered to negative pitch angles at very high depths in the corona to form the electrons returning back to the injection site. These returning beam electrons substitute in a return current the ambient electrons, and their contribution significantly increases with the precipitation depth.

On the other hand, lower energy electrons lose much more energy in a joint effect of self-induced field and collisions compared to pure collisions, which results in fewer lower energy electrons and hard X-ray photon spectra of a broken power law type (Zharkova & Gordovskyy 2005). The higher the beam energy flux and the higher its spectral index, the bigger the difference between the spectral indices of lower and higher energy parts in HXR photon spectra (Zharkova & Gordovskyy 2005). However, in these previous numerical kinetic solutions we did not separate the effects of a self-induced electric field from collisions and anisotropic scattering and thus, were not clear what mechanisms are responsible for the features observed in HXR emission. Moreover, the recent electron mean spectra with dips at lower energies deduced from the *RHESSI* observation (Massone et al. 2004) have provided additional restrictions on electron beam kinetics and required a revised study of the effect of a self-induced electric field.

Hence, the motivation of the current research is to obtain analytical kinetic solutions in a pure electric field for collisionless precipitation of electron beams into the ambient plasma, to compare them with pure collisions and to revise the full kinetic results (Zharkova & Gordovskyy 2005) in light of these solutions in order to interpret the observed patterns in HXR photon and mean electron spectra. The kinetic solutions for pure electric and combined energy losses are described in § 2, the resulting electron, mean, and photon energy spectra are discussed in § 3, and conclusions are drawn in § 4.

2. THE PROBLEM DESCRIPTION

2.1. *Distribution Function for Beam Electrons*

Let us consider electron beam precipitation from a source in the corona (depth $x_{\min}$) downward to the photosphere (depth $x_{\max}$) (a one-dimensional atmosphere). The ambient plasma conditions (temperature T, density n, and macrovelocities V) are assumed to vary with depth according to the hydrodynamic response of the ambient plasma to electron beam injection (Somov et al. 1981, 1982; Nagai & Emslie 1984) and as plotted in Figure 1 (Zharkova et al. 1995). The ionization degree X at chromospheric levels is assumed to be governed by the non-LTE ionization balance of hydrogen atoms (Zharkova & Kobylinskii 1993).

During this precipitation the electron beam can be described by a distribution function $f = f(x,\ E,\ \theta)$ in the phase space, where x is precipitation depth, E is energy, and θ is a pitch angle, i.e., the angle between the electron velocity vector and the magnetic field direction. The distribution function is normalized with a scaling factor K (to the initial total energy flux F_0 of the beam particles at injection on the top boundary in the corona in ergs cm^{-2} s^{-1}) for a given range of energy and pitch angles as follows:

$$F_0 = K \int_{x_{\min}}^{x_{\max}} \int_{E_{\rm low}}^{\infty} \int_{-1}^{1} E^{3/2} f(x,\ E,\ \theta)\, dE\, d\mu\, dx, \qquad (1)$$

where $E_{\rm low}$ is a lower energy cutoff and $\mu = \cos\theta$. Then the scaling factor K can be defined from the initial energy flux F_0 for any spectral index γ (Zharkova & Gordovskyy 2005).

2.2. *Description of the Problem*

We take into account two forms of electron energy losses: collisions with the ambient plasma particles and deceleration in the self-induced electric field. The electron beam kinetics with pitch-angle deflection can be described by the Fokker-Planck, or Landau, kinetic equation (Zharkova & Gordovskyy 2005):

$$\mu \frac{\partial f}{\partial x} = e\mathcal{E}\mu \frac{\partial f}{\partial E} + \frac{e\mathcal{E}}{2E}\left(1-\mu^2\right)\frac{\partial f}{\partial \mu} + \left(\frac{\partial f}{\partial x}\right)_{\rm coll}, \qquad (2)$$

where f is the electron beam distribution function and e and m_e are the electron charge and mass, respectively. Here $\mathcal{E}$ is the self-induced electric field at a given depth x that can be written as follows:

$$\mathcal{E}(x) = \frac{2\sqrt{2}\pi}{\sigma(x)} \frac{e}{\sqrt{m_e}} \int_0^{\infty} \int_{-1}^{1} f(x,\ E,\ \theta)\sqrt{E}\mu\, dE\, d\mu, \qquad (3)$$

where $\sigma(x)$ is the ambient plasma classic conductivity (see, e.g., Benz 2002, p. 216).

The term $(\partial f/\partial x)_{\rm coll}$ on the right-hand side describes particle energy losses and pitch-angle diffusion caused by collisions with the ambient plasma particles, or a collisional integral, taken in the linearized form (Diakonov & Somov 1988):

$$\left(\frac{\partial f}{\partial x}\right)_{\rm coll} = \frac{m_e^{2.5}}{4E}\frac{\partial}{\partial E}\left[\frac{\nu(E)}{\sqrt{E}}\left(k_{\rm B}T_e\frac{\partial f}{\partial E} + f\right)\right] + \nu(E)\frac{\partial}{\partial \mu}\left[\left(1-\mu^2\right)\frac{\partial f}{\partial \mu}\right]. \qquad (4)$$

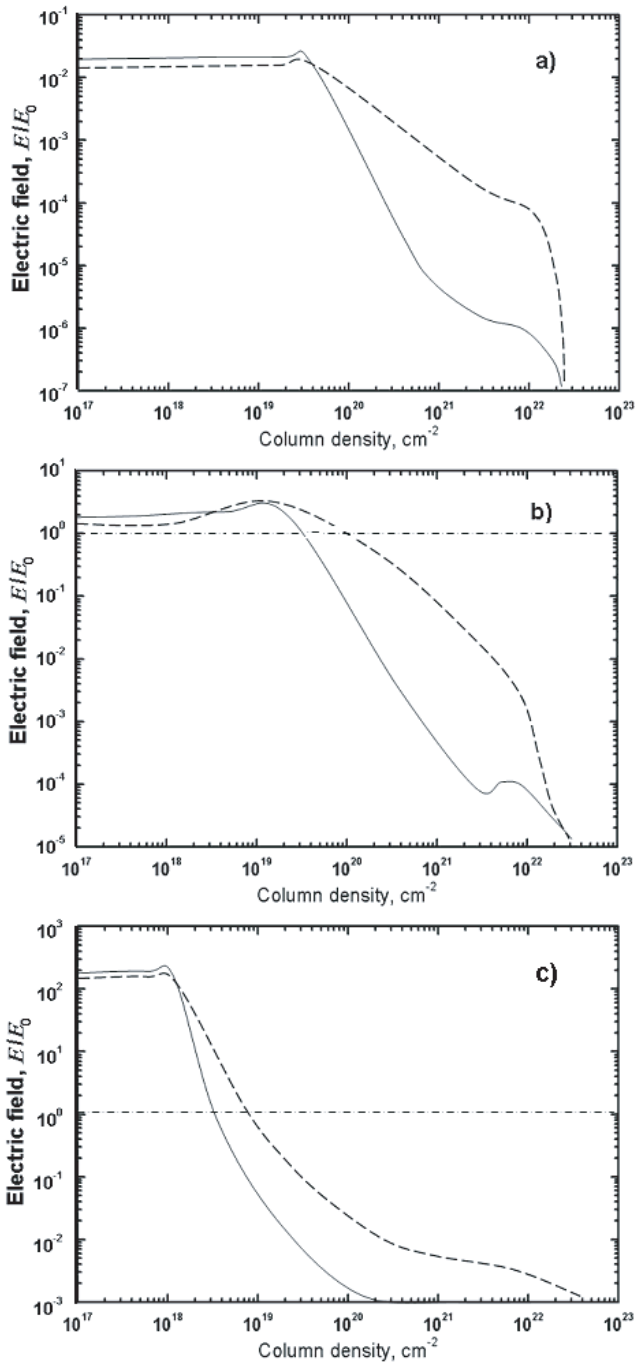

FIG. 1.—Electric field induced by electron beams with $\gamma = 3$ (*dashed lines*) and 7 (*solid lines*) and the initial energy flux of $F_0 = 10^8$ ergs cm^{-2} s^{-1} (*a*), $F_0 = 10^{10}$ ergs cm^{-2} s^{-1} (*b*), and $F_0 = 10^{12}$ ergs cm^{-2} s^{-1} (*c*) (from the simulations by Zharkova & Gordovskyy 2005).

The first term defines energy diffusion of beam electrons, the second accounts for beam energy losses in collisions, and the third takes into account the pitch-angle diffusion.

The injected beam is assumed to have a power-law energy spectrum in the energy range from $E_{\rm low}$ to $E_{\rm upp}$ with a spectral index γ and normal distribution in a pitch-angle cosine with the half-width dispersion $\Delta\mu = 0.2$ per equation (13) of Zharkova & Gordovskyy (2005). It has to be noted that the exact form of the initial pitch-angle distributions at injection is not crucial for the kinetic solutions (Zharkova et al. 1995). In order to concentrate on the electric field effect, the kinetic equation was solved numerically for beam electrons with spectral indices of 3, 5, and 7 and initial energy fluxes of 10^8, 10^{10}, and 10^{12} ergs cm^{-2} s^{-1} precipitating in a constant magnetic field (Gordovskyy & Zharkova 2003; Zharkova & Gordovskyy 2005) with low-energy cutoff $E_{\rm low} = 8$ keV and high-energy cutoff $E_{\rm upp} = 384$ keV.

2.3. *The Mean Electron Flux Spectra*

For isotropic photon emission, i.e., for the HXR emission cross sections being not dependent on pitch angles of the scattered electrons and photons, the mean electron flux can be defined by the expression (see Brown et al. 2003)

$$\bar{\mathcal{F}}(E) = K \int_{\xi} \int_{\mu} f(\xi,\ E,\ \mu) E^{1/2}\, d\mu\, d\xi, \qquad (5)$$

where f is the distribution functions from equation (2), n is the ambient plasma density, and ξ is the column depth $\xi = \int_{x_{\rm min}}^{x_{\rm max}} n(x)\, dx$.

The function $\bar{\mathcal{F}}(E)$ is essential for understanding the photon spectra because it can be deduced by inversion of the observed spectra without any additional assumptions about the conditions in the target (Brown et al. 2003). This approach is valid for mean pitch-angle scattering when the HXR photon cross sections are not dependent on pitch angles, which is not always the case in solar flares (Brown 1971; Zharkova et al. 1995; Massone et al. 2004; Zharkova & Gordovskyy 2005).

2.4. *The Hard X-Ray Bremsstrahlung Emission*

The resulting hard X-ray bremsstrahlung emission produced in the magnetic field direction is

$$\frac{dI(h\nu)}{d(h\nu)} = CK \int_{\xi} \int_{h\nu}^{\infty} \int_{\mu} f(\xi, E, \mu) E^{3/2} \sigma^{B}(E, h\nu, \mu)\, d\mu\, dE\, d\xi, \qquad (6)$$

where $h\nu$ is the photon energy, E is the electron energy, σ^B is the bremsstrahlung differential cross section in the direction parallel to the magnetic field (see Haug 1997), and C is the scaling constant taking into account an area on the solar surface covered by a flaring atmosphere, the dilution factor associated with the Sun-to-Earth distance, and some physical constants (Zharkova & Gordovskyy 2005).

3. RESULTS AND DISCUSSION

3.1. *Depth Distributions of a Self-induced Electric Field*

The kinetics of very intense electron beams can be strongly affected by the self-induced electric field (Zharkova et al. 1995; Zharkova & Gordovskyy 2005). The electric field distributions with depth found from the full kinetic simulations by Zharkova & Gordovskyy (2005) are plotted in Figure 1 for electron beams with $\gamma = 3$ and the initial flux of 10^8 ergs cm^{-2} s^{-1} (*top*), 10^{10} (*middle*), and 10^{12} (*bottom*) (Zharkova & Gordovskyy 2005). The electric field is measured in units of the local Dreicer field induced by the ambient plasma particles at a given depth, i.e., $\mathcal{E}_{\rm D} = 2\pi e^3 n \ln\Lambda/(k_{\rm B}T)$, where $T(\xi)$ and $n(\xi)$ are the local temperature and density and $\ln\Lambda$ is the Coloumb logarithm. For weak hard beams ($F_0 = 10^8$ ergs cm^{-2} s^{-1}, $\gamma = 2$–3), the induced field is weaker (10^{-7} V cm^{-1}) than the local Dreicer field, while for the intense softer beams (10^{11}–10^{12} ergs cm^{-2} s^{-1}), it can reach 10^{-3} V cm^{-1}, which is comparable or even higher than $\mathcal{E}_{\rm D}$ by a factor of 10–100.

The self-induced electric field related directly to the precipitating beam density (see eq. [3]) is found to be nearly constant at upper coronal levels and to strongly decrease with depth in the

TABLE 1
"Stopping" Column Depths

E (keV)	ξ_{max} (cm^{-2}) $a = 2.7\times10^{-12}$ eV^2 cm^2	$\mathcal{E} = 10^{-5}$ V cm^{-1}	$\mathcal{E} = 10^{-4}$ V cm^{-1}	$\mathcal{E} = 10^{-3}$ V cm^{-1}
10	1.8×10^{19}	3.2×10^{19}	3.5×10^{17}	2.2×10^{17}
40	2.9×10^{20}	$>10^{25}$	1.6×10^{18}	2.6×10^{17}
100	1.8×10^{21}	$>10^{25}$	3.2×10^{19}	3.5×10^{17}
400	2.9×10^{22}	$>10^{25}$	$>10^{25}$	1.6×10^{18}

Note.—Comparison of the "stopping" column depths for electrons with different energies (first column) for pure collisional losses (second column) or for pure electric field losses (last three columns).

lower corona and transition region (see Fig. 1). For weaker hard beams the induced electric field is nearly constant until a column depth of a few times 10^{20} cm^{-2} (the upper chromosphere) and then smoothly decreases toward the photosphere (Fig. 1*a*). For more intense hard beams the magnitude of the constant electric field increases proportionally to the initial flux but remains constant only at levels of 10^{19} cm^{-2} (for initial flux of 10^{10} ergs cm^{-2} s^{-1}) (Fig. 1*b*) or even 10^{18} cm^{-2} (for 10^{12} ergs cm^{-2} s^{-1}; Fig. 1*c*), after which it sharply drops. The rate of decrease depends on the beam spectral index being steeper for softer beams (5–7) than for harder ones (3), as shown by the solid and dashed lines in Figures 1*a*–1*c*.

Therefore, the induced electric field is constant only in higher atmospheric levels after the beam injection but throughout the most flaring atmosphere it is variable falling with depth x exponentially, i.e., linearly (x^{-1}), parabolically (x^{-2}), or steeper (x^{-k}) (see Fig. 1). The "turning" depth, where the electric field starts decreasing, is very important for understanding the resulting electron beam kinetics, as we show below.

3.2. *Kinetic Solutions for a Pure Electric Field*

In order to understand the effect of an electric field, let us consider the kinetics of a beam governed only by the energy losses in a pure electric field $\mathcal{E}$. Let us assume that during precipitation of a power-law electron beam there is an electric field, constant or variable, that is not affected by the precipitating beam (no collisions or pitch-angle scattering). For the sake of simplicity, let us also assume that the beam is injected in the direction $\mu = 1$ with δ-like pitch angular distribution and that the particles can either precipitate downward ($\mu = 1$) or, after they fully lose their energy, move backward to the source in the corona ($\mu = -1$).

3.2.1. *Energy Losses in Electric Field*

Let us consider the energy losses in a pure electric field (Emslie 1980):

$$\frac{dE}{\mu\, dx} = -e\mathcal{E}, \tag{7}$$

where x is the linear precipitation depth.

Obviously, lower energy electrons lose their energy at higher atmospheric levels than more energetic ones. Let us introduce an "electric" stopping depth $x_{\mathcal{E}}$, at which the electron with energy E loses it completely; i.e.,

$$x_{\mathcal{E}} = \frac{E}{\mu e\mathcal{E}}, \qquad \text{or } \xi_{\mathcal{E}} \approx \frac{nE}{\mu e\mathcal{E}}. \tag{8}$$

For example, for an electric field of 10^{-3} V cm^{-1}, electrons with initial energies of 30 and 300 keV lose their energy completely at the associated "electric" column depths of 5×10^{17} and 6×10^{23} cm^{-2}, respectively, for the atmosphere described in § 2.1. Hence, depending on the strength of the electric field $\mathcal{E}$, the "electric" stopping column depth can be much shorter than the collisional one. This leads to lower energy beam electrons to start returning to the injection source in the corona from much higher atmospheric depths than those where they would fully lose their energy in collisions.

In Table 1 we present a comparison of the "collisional" and "electric" stopping depths calculated for the electric field magnitudes relevant for the accepted beam parameters and the exponential atmospheres considered. From Table 1 we can conclude that intense softer beams inducing higher electric fields have their electric stopping depths located very high in the corona ($\leq 10^{18}$ cm^{-2}), which is close to the injection source (10^{17} cm^{-2}).

3.2.2. *Continuity Equation*

The electron beam differential density (per depth and energy unit) in the flaring atmosphere can be found from the continuity equation (Syrovatskii & Shmeleva 1972):

$$\frac{\partial}{\partial x}[VN(x,\ E)] + \frac{\partial}{\partial E}\left[\left(\frac{dE}{dx}\right)VN(x,\ E)\right] = 0. \tag{9}$$

Let us assume that the initial beam spectrum is a power law in energy with the spectral index for the flux γ giving the initial electron density as

$$N(E,\ 0) = KE^{-\gamma-0.5}\Theta(E - E_{\rm low}) \tag{10}$$

and seek analytical solutions of equation (9) for constant and variable electric fields.

3.2.3. *Constant Electric Field*

For a constant electric field ($\mathcal{E} = \mathcal{E}_0$) the beam differential densities can be found analytically from the continuity equation using the same method as in Syrovatskii & Shmeleva (1972) with the energy losses taken from equation (8):

$$N(E,\ x) = K\mathcal{E}_0^{-0.5}(E + e\mathcal{E}_0x)^{-\gamma}\Theta(E - E_{\rm low} + e\mathcal{E}_0x) \times \Theta(E_{\rm upp} - e\mathcal{E}_0x - E), \quad \text{for } \mu = +1, \tag{11}$$

$$N(E,\ x) = K\mathcal{E}_0^{-0.5}(e\mathcal{E}_0x)^{-\gamma}\Theta(E - E_{\rm low} - e\mathcal{E}_0x) \times \Theta(E_{\rm upp} + e\mathcal{E}_0x - E), \quad \text{for } \mu = -1. \tag{12}$$

The differential spectra above are asymmetric for precipitating ($\mu = 1$) and for returning ($\mu = -1$) particles, as is illustrated by Figure 2 for electron beams with the initial flux of 10^8 and

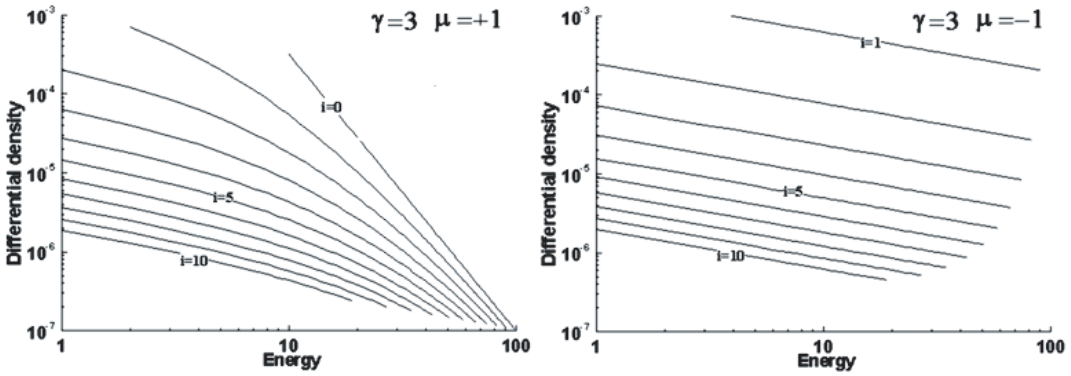

FIG. 2.—Differential densities found in a pure electric field approach for precipitating electrons (*left*) and returning electrons (*right*) from the continuity equation for a beam with $\gamma = 3$ and an electric field magnitude of 5×10^{-5} V cm^{-1}. The depths of beam precipitation are calculated according to the numbers i as $x_i = 1.6 \times 10^8 i$ cm.

10^{12} ergs cm^{-2} s^{-1} and initial index $\gamma = 3$ (*left*; for $\mu = 1$, *right*; for $\mu = -1$). After completely losing their energy in the electric field while precipitating downward to the photosphere, the electrons become accelerated by this field in the opposite direction and return back to the source on the top; let us call these returning electrons. The energy gained by the returning electrons during the acceleration depends on their original energy, or their stopping depth, from which they start their way back to the source. This depth is smaller for lower energy electrons and larger for higher energy ones, as demonstrated by Figure 2 for $\mu = -1$.

The differential densities of precipitating electrons depend on the linear precipitation depth x that can be associated with a column depth and the ambient plasma density as $x \simeq \xi/n$. As expected, for a constant electric field in the atmosphere with density exponentially increasing with a precipitating distance x, the beam electrons steadily lose the same amount $e\mathcal{E}x$ of their energy. For lower energy electrons, with every step of their precipitation their loss becomes more noticeable compared to their energy. Therefore, at deeper atmospheric layers the electron differential spectra at lower energies steadily decrease and become flatter, until all electrons are fully decelerated by the electric field (see Fig. 2 for $\mu = 1$). Hence, unlike the electron spectra for pure collisional losses, which are dependent only on column depth, the distributions of beam electron densities in an electric field is dependent on the linear depth.

3.2.4. *Variable and Combined Electric Field*

As discussed in § 3.1, the induced electric field found from the full kinetic solutions is mostly variable in a flaring atmosphere being a constant only at higher atmospheric levels, after which it falls exponentially (linearly, parabolically, or steeper; see Fig. 1 above).

Let us obtain the pure electric solutions for a few cases of Ohmic energy losses in an electric field varying with depth as $\mathcal{E} = \mathcal{E}_0(x/x_t + 1)^{-k}$, where $\mathcal{E}_0$ is a constant electric field (the magnitude at the injection), x_t is the turning depth where the electric field starts decreasing, and $x \geq x_t$.

For $k = 1$ the differential spectra of precipitating beam electrons can be written as

$$N(E,\ x) = \frac{K}{\sqrt{E}}\left(E + e\mathcal{E}_0 x_t \ln\frac{x}{x_t}\right)^{-\gamma}\Theta\left(E - E_{\rm low} + e\mathcal{E}_0 x_t \ln\frac{x}{x_t}\right) \times \Theta\left(E_{\rm upp} - e\mathcal{E}_0 x_t \ln\frac{x}{x_t} - E\right); \quad (13)$$

for $k \geq 1$ they can be defined as follows:

$$N(E,\ x) = \frac{K}{\sqrt{E}}\left(E + \frac{e\mathcal{E}_0 x_t}{k-1}\left[1 - \left(\frac{x}{x_t}\right)^{1-k}\right]\right)^{-\gamma} \times \Theta\left(E - E_{\rm low} + \frac{e\mathcal{E}_0 x_t}{k-1}\left[1 - \left(\frac{x}{x_t}\right)^{1-k}\right]\right) \times \Theta\left(\left\{E_{\rm upp} - \frac{e\mathcal{E}_0 x_t}{k-1}\left[1 - \left(\frac{x}{x_t}\right)^{1-k}\right] - E\right\}\right). \quad (14)$$

The precipitating electrons, whose "electric" stopping depth is below the depth of the electric field turning point, will lose less of their energy in deceleration by a decreasing electric field than in the constant one. This will result in smaller flattening of the differential energy spectra for the variable (decreasing) electric field, as demonstrated in Figure 3 for the beam with initial flux of 10^{12} ergs cm^{-2} s^{-1} and $\gamma = 3$, where the electric field is assumed to be either a constant (*a*) or decreasing as $\sim x^{-1}$ (*b*) and $\sim x^{-2}$ (*c*).

In Figure 4 the differential spectra are plotted for a combined electric field with the turning point occurring at step 4 ($i = 4$ on the plots in Fig. 4) for the electric field decrease as $\sim x^{-1}$ (*a*), $\sim x^{-2}$ (*b*), and $\sim x^{-5}$ (*c*). It can be seen that precipitating electrons with higher energies, whose "electric" stopping depth is deeper than the turning point, suddenly become less decelerated because of the decreasing electric field, and, as result, they can precipitate much deeper. Hence, a decrease of the electric field leads to a smaller energy loss by electrons and to smaller flattening of their differential spectra in comparison with the constant electric field.

In Figure 5 the differential spectra are plotted for a combined electric field with the turning point occurring at step 4. The constant part of electric field $\mathcal{E}_0$ is accepted to range from 5×10^{-5} (*a*) to 4×10^{-4} V cm^{-1} (*b*), corresponding to the magnitudes from Figure 1, and the variable part decreases with depth as $\sim x^{-2}$. It can be noted that for a higher electric field $\mathcal{E}_0$ there is a much faster decrease in the electron numbers at lower energies and, as result, larger flattening in their differential spectra.

3.2.5. *Mean Electron Flux Spectra from the Source*

Constant electric field.—Let us calculate the mean electron flux spectra obtained from beam electrons precipitating in a constant electric field by integrating the differential spectra in

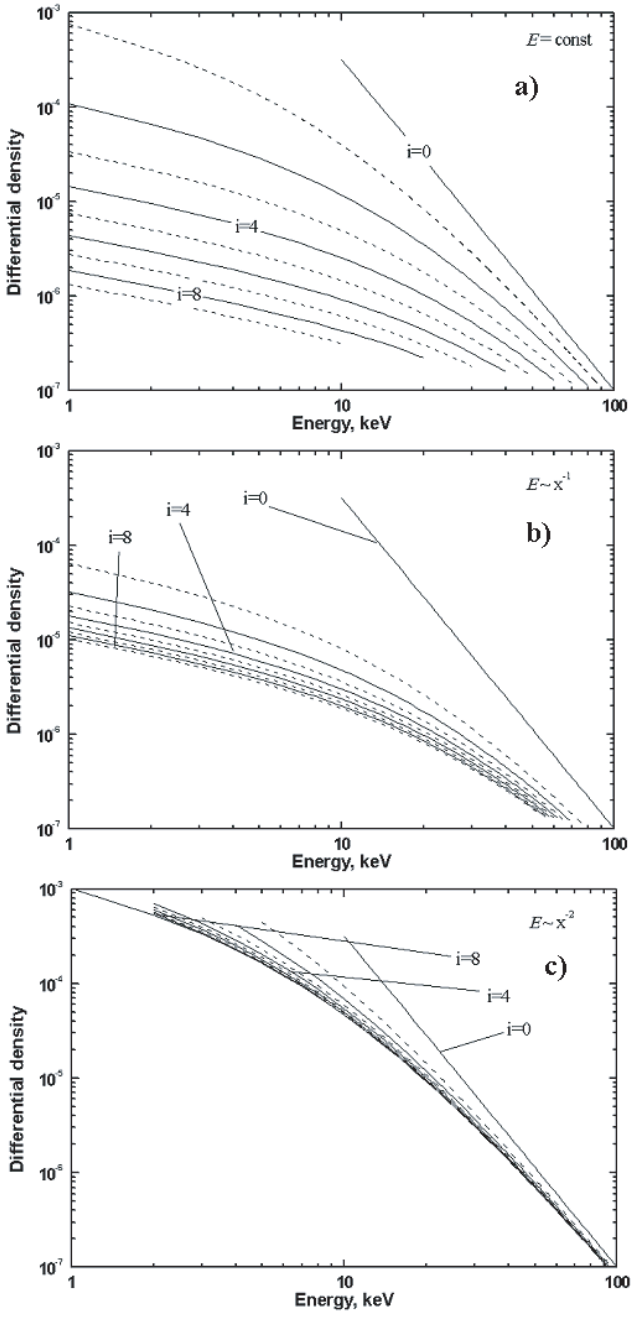

FIG. 3.—Differential spectra of beam electrons with $\gamma = 3$ calculated in a pure electric approach for a constant field (5×10^{-5} V cm^{-1}) (*a*) and for an electric field decreasing as $1/x$ (*b*) and $1/x^2$ (*c*). The depths of beam precipitation are calculated as in Fig. 2.

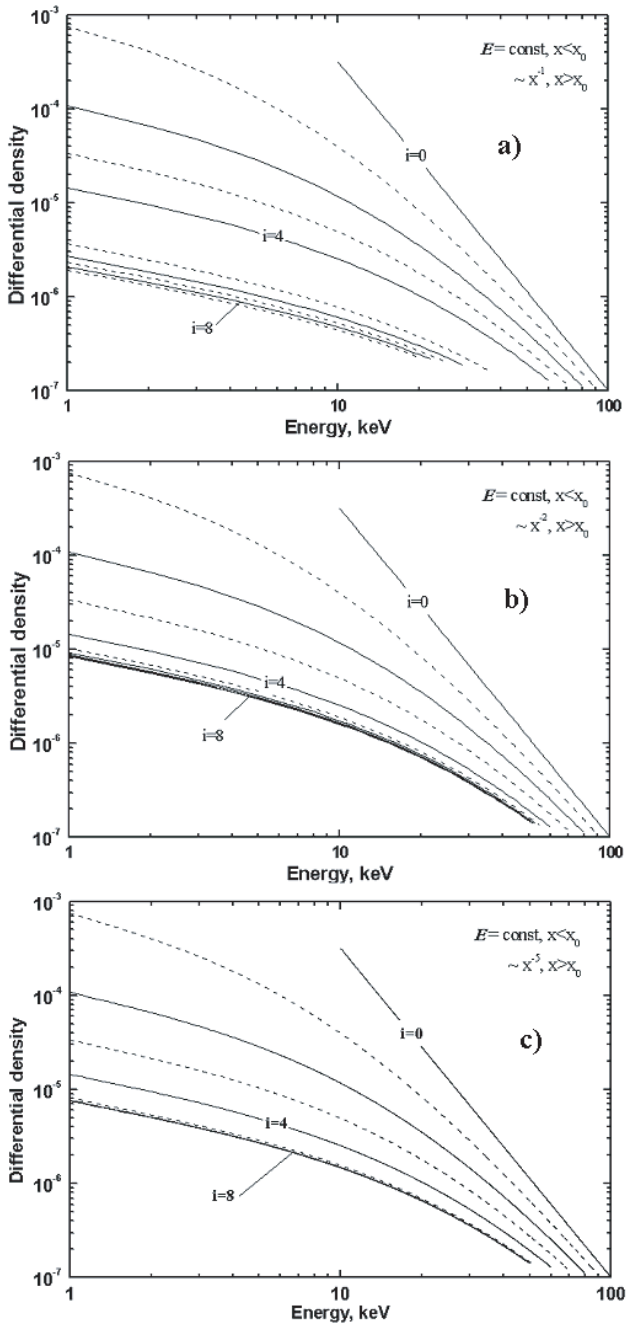

FIG. 4.—Differential spectra of beam electrons with $\gamma = 3$ calculated in a pure electric approach for a combined electric field with a constant part of 5×10^{-5} V cm^{-1}, turning point at $i = 4$, and with a variable field dropping as $1/x$ (a), $1/x^2$ (*b*), and $1/x^5$ (*c*). The depths of beam precipitation are calculated as in Fig. 2.

equation (5) (§ 3.2.3) over the depth range from 0 to infinity as follows:

$$\bar{\mathcal{F}}(E) = \sqrt{\frac{2}{m_e}} K \frac{\gamma - 1}{e\mathcal{E}} E^{-\gamma+1} \sim E^{-\beta_E}. \qquad (15)$$

The mean electron flux spectra of electron beams with the initial energy flux of 5×10^{10} ergs cm^{-2} s^{-1} and spectral index $\gamma = 3$ are plotted in Figure 6*a* (curve 1) for the constant electric field magnitude of 5×10^{-5} V cm^{-1}.

It can be noted that for a constant electric field the spectral index β_E is related to the initial spectral index γ of the beam electrons as

$$\beta_E \simeq \gamma - 1, \qquad (16)$$

which is different by 1 from $\beta = \gamma - 2$ found for pure collisions (Syrovatskii & Shmeleva 1972; Brown et al. 2003).

Variable electric field.—By repeating the procedure above for the depth range between $x_{\min}$ and $x_{\max}$ with the differential densities from § 3.2.4, we can obtain the mean electron flux

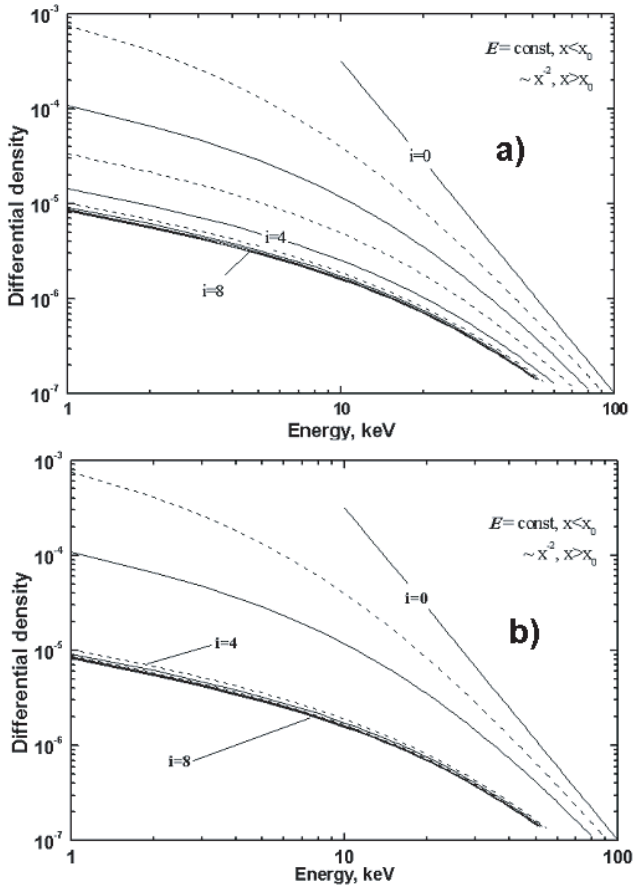

FIG. 5.—Differential spectra of beam electrons with $\gamma = 3$ calculated in a pure electric approach for a combined electric field falling as $1/x^2$ with turning point at $i = 4$ and with a constant part of 5×10^{-5} V cm^{-1} (*a*) and 4×10^{-4} V cm^{-1} (*b*). The depths of beam precipitation are calculated as in Fig. 2.

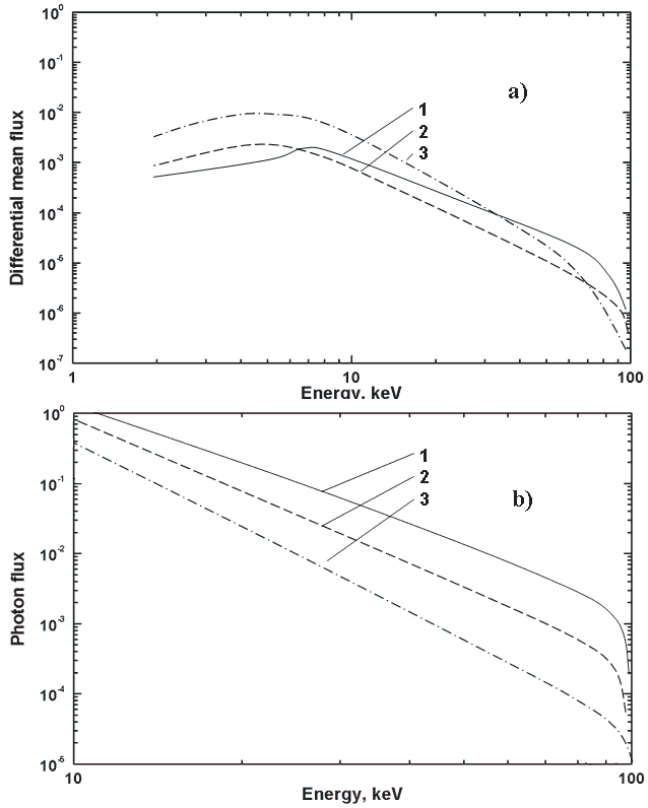

FIG. 6.—Mean electron fluxes and photon spectra in a pure electric field approach for the differential spectra from Fig. 2.

spectra for electrons in a variable electric field presented in Figures 6*a*–6*b*. The mean electron fluxes are calculated for the beams with $\gamma = 3$ in a variable electric field decreasing as $\sim x^{-1}$ (curve 2) and as $\sim x^{-2}$ (curve 3). For the field decreasing as $\sim x^{-1}$, the mean flux index $\beta = \gamma - 0.6 = 2.4$, and for the electric field decreasing as $\sim x^{-2}$, $\beta = \gamma - 0.1 = 2.9$.

Combined electric field.—For a combined electric field, i.e., constant before the turning depth x_t, or ξ_t, somewhere in the corona (at the fourth depth point, for example) and decreasing afterward, the differential spectra in the constant part are defined from § 3.2.3 and for the electric field decreasing with depth as $\sim x^{-k}$ the differential spectra defined from § 3.2.4. Then by performing the numerical integration within the limits $x_{\min}$ and $x_{\max}$, we obtain the mean electron flux spectra for a combined electric field.

The results are presented in Figure 7*a* for the same electric field variations as in Figure 4: constant at 5×10^{-5} V cm^{-1} until depth of 4 and decreasing as $\sim x^{-1}$ (curve 1), $\sim x^{-2}$ (curve 2), or $\sim x^{-5}$ (curve 3). The resulting mean electron flux distributions show a stronger spectra flattening toward lower energies for those electric fields, which decrease faster with depth (compare curve 1 with 2 and 3), reflecting higher energy losses in electric field for lower energy particles, as discussed in § 3.2.4.

3.2.6. *Photon Spectra*

Constant electric field.—By substituting the solutions for differential spectra from § 3.2.3 into equation (6) and using the

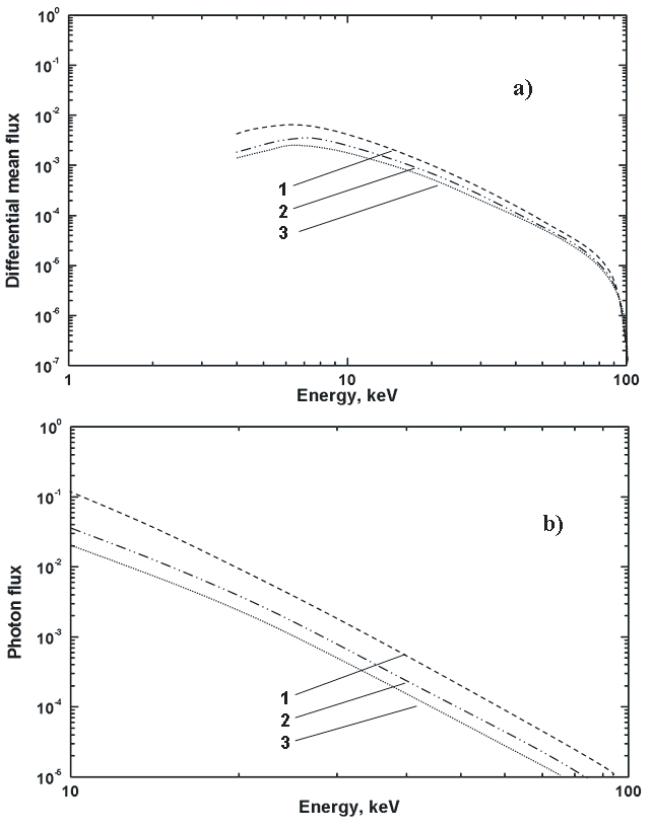

FIG. 7.—Mean electron fluxes and photon spectra in pure electric field approach for the differential spectra from Fig. 4.

classic nonrelativistic cross sections for HXR emission in the Borne approximation (Lang 1974), the photon fluxes for pure electric solutions can be obtained analytically as

$$\frac{dI(h\nu)}{d\nu} = \frac{K}{(\gamma-1)e\mathcal{E}}(h\nu)^{-\gamma} \sim h\nu^{-\delta}. \quad (17)$$

The photon fluxes from beam electrons precipitating in a constant electric field are also power laws with spectral index δ equal to the spectral index γ of the initial electron beam (see Fig. 7*b*, curve 1). This is different from the pure collisional case when the photon flux spectra index $\delta = \gamma - 1$ (Syrovatskii & Shmeleva 1972; Zharkova & Gordovskyy 2005).

Combined electric field.—Photon spectra produced by electron beams propagating in a variable electric field calculated from the differential spectra in § 3.2.4 for the HXR cross sections of Haug (1997) are presented in Figure 7*b*. The photon spectra are calculated for the same HXR cross section for beam electrons with $\gamma = 3$ with the differential spectra plotted in Figure 4. The electric field is assumed to be constant of 5×10^{-5} V cm^{-1} in depth points 1–4 and from depth point 5 decreasing as $\sim x^{-1}$ (curve 1) or as $\sim x^{-2}$ (curve 2) and $\sim x^{-5}$ (curve 3).

The spectral indices of photon spectra at lower energies are close to $\delta_{\rm low} = 2.8$ (curves 1–3) that is slightly lower than the electron index of 3. On the other hand, the photon spectral indices at higher energies, $\delta_{\rm high} = 3.5$–4.3, increasing faster for the steeper decrease of electric field (compare the curve 1 for $\sim x^{-1}$, the curve 2 for $\sim x^{-2}$ and the curve 3 for $\sim x^{-5}$). It can be deduced that the decrease of a variable electric field as $\sim x^{-k}$ leads to an increase of the photon spectral indices approximately as $\delta \approx \gamma + k/(k+1)$.

Hence, the combined (constant plus decreasing) electric field can lead to a noticeable hardening in the photon spectra at lower energies and softening at higher ones. This can be explained by the fact that in the combined electric field, beam electrons are first decelerated by a constant electric field. The magnitude of this deceleration is proportional to the initial energy flux of the precipitating electron beam leading to a substantial decrease (proportional to this flux) of the photon flux indices at lower energies. However, starting from the turning point the beam electrons become less and less decelerated by the electric field, as discussed in § 3.2.4. This will lead to a smaller flattening at lower energies of their differential spectra and to the photon spectra indices being higher than the electron beam ones, as established in § 3.2.6.

3.3. *The Full Kinetic Solutions*

These analytical solutions can help us to understand better the numerical ones found from the full kinetic equation taking into account anisotropic scattering in collisions in the presence of both magnetic and self-induced electric fields.

3.3.1. *Energy and Pitch-Angle Variations with Depth*

In this case, the energy losses are dependent on the electron energies, their pitch angles or cosines, $\mu = \sin\theta$, and the induced electric field as (Emslie 1980; Zharkova et al. 1995; Zharkova & Gordovskyy 2005)

$$\frac{dz}{\mu d\xi} = -\frac{2}{\mu z}\left[X + (1-X)\frac{\ln\Lambda'}{\ln\Lambda}\right] - 2\varepsilon, \quad (18)$$

and pitch-angle cosines of the beam electrons scattered in a presence of the self-induced electric field ε and a converging magnetic field vary as

$$\frac{d\mu}{d\xi} = -\frac{1}{z^2}\left[2X + (1-X)\frac{\ln\Lambda' - \ln\Lambda''}{\ln\Lambda}\right] - \frac{1-\mu^2}{\mu z}\varepsilon + \left(\frac{d\mu}{d\xi}\right)_{\rm magn}, \quad (19)$$

where μ is the pitch-angle cosine, z is a dimensionless energy $z = E/E_{\rm low}$, $E_{\rm low}$ is the lower cutoff energy, ξ is a precipitation column depth, X is the ionization degree, and $(d\mu/d\xi)_{\rm magn}$ are the pitch-angle cosine changes caused by the converging magnetic field B. The dimensionless electric field is defined as $\varepsilon = \mathcal{E}/\mathcal{E}_0$, $\mathcal{E}_0 = 2\pi n \ln\Lambda/E_{\rm low}$, n is the ambient plasma density, and $\ln\Lambda$, $\ln\Lambda'$, and $\ln\Lambda''$ are the Coulomb logarithms for electrons, protons, and neutral hydrogen atoms, respectively.

The pitch-angle cosine changes caused by the converging magnetic field B are described as:

$$\left(\frac{d\mu}{d\xi}\right)_{\rm magn} = -\frac{1}{2}(1-\mu^2)\frac{\partial lnB}{\partial\xi} \quad \text{or}$$
$$\left(\frac{d\mu}{d\xi}\right)_{\rm magn} = \frac{1}{2}\mu\sqrt{1-\mu^2}\frac{\partial lnB}{\partial\xi}, \quad (20)$$

where the left-hand side of equation (20) describes the particles that are mirrored by the converging magnetic field with pitch angles $\theta \geq \sin^{-1}(B_{\rm min}/B_{\rm max})^{1/2}$ and the right-hand side defines those that precipitate within the loss cone, i.e., with pitch angles $\theta < \sin^{-1}(B_{\rm min}/B_{\rm max})^{1/2}$.

If the dimensionless electric field $\varepsilon < E_{\rm low}/E\mu$, then the energy losses are mostly caused by collisions (term 1 in eq. [18]) and, if $\varepsilon \geq E_{\rm low}/E\mu$, then the electric field losses (term 2) will dominate. Owing to both collisions and electric field to E', the initial electron energy E at injection will change with a precipitation depth ξ as

$$E' = \sqrt{E^2 - 2a\xi} - \frac{e\mathcal{E}\xi}{n}. \quad (21)$$

The change in μ for an electron due to collisional scattering (the first term in eq. [19]) varies inversely with the square of the electron energy. The change due to Ohmic losses (second term) is proportional to the magnitude of the electric field and inversely proportional to the electron energy. The change in a converging magnetic field (third term) depends only on the magnetic field convergence, not on the energy or the electric field.

The second term of equation (19) is negative for $\mu > 0$, so the effect of the self-induced electric field is to decrease μ (increasing the pitch angle) and eventually to turn the electron around. This negative value of μ can only be achieved if the electron energy is comparable to or lower than the energy of the electric field ($e\mathcal{E}$). This condition becomes valid for more electrons as the depth increases.

The third term of equation (19) is either negative or positive (see eq. [20]) depending on the magnetic convergence; i.e., it is positive for the electrons moving within the loss cone with pitch angles $\theta_{\rm cone} < \sin^{-1}(B_{\rm min}/B_{\rm max})^{1/2}$ and is negative for larger pitch angles leading to particle mirroring. At upper atmospheric depths in the corona the magnetic mirroring of electrons becomes effective for the particles with the pitch angles bigger than $\theta_{\rm cone}$. These particles can also contribute to the returning electrons and, in the loop with two footpoints, can be trapped.

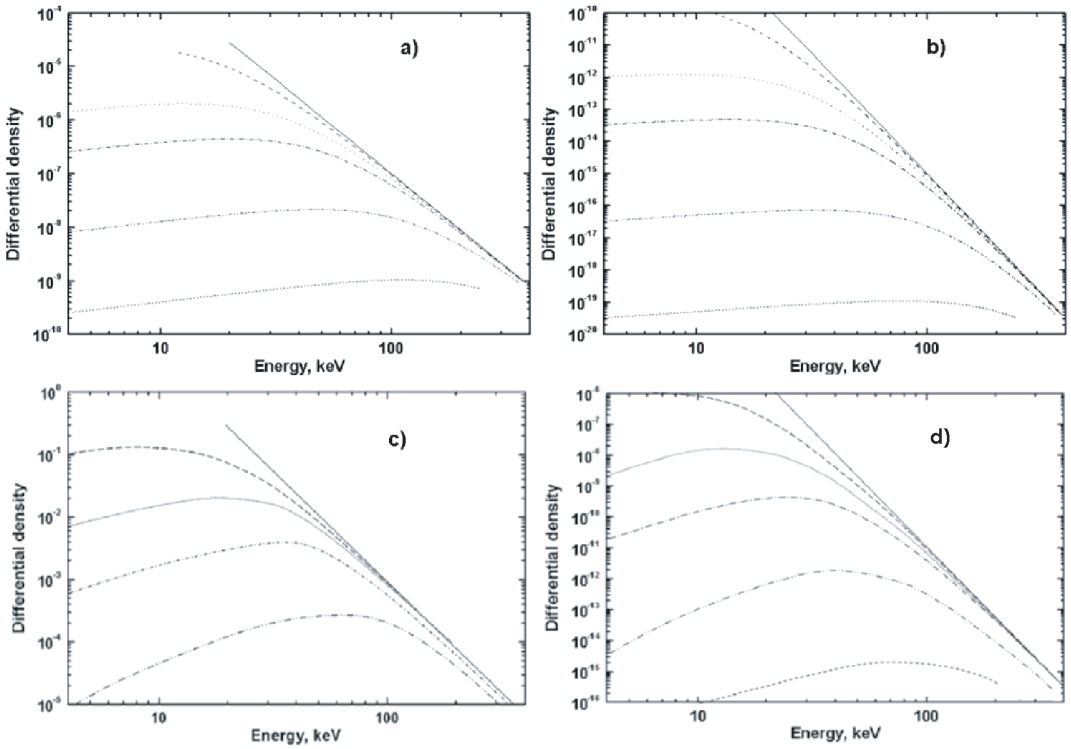

FIG. 8.—Differential spectra for a full kinetic approach calculated for beams with the initial energy fluxes of 10^8 (*top panels*) and 10^{12} ergs cm^{-2} s^{-1} (*bottom panels*) for $\gamma = 3$ (*left panels*) and 7 (*right panels*).

However, even in the mirror regime collisions continuously scatter trapped particles into the loss cone, giving rise to a slow leakage of plasma out of the magnetic mirror. Moreover, plasmas with power-law distribution functions are prone to velocity space instabilities, which tend to relax the distribution function back to a Maxwellian one. But these effects are not considered in the current study and will be done in a future paper.

Therefore, if particles are scattered by collisions within the loss cone in a presence of the converging magnetic field and the self-induced electric field (acting in the opposite direction to their movement), their pitch angles are affected in different ways. The self-induced electric field works to turn the electrons to the pitch angles larger than $\pi/2$ trying to keep them moving along the electric field direction. This can be achieved only when the electron energy is comparable to or lower than the energy of the electric field ($e\mathcal{E}$), which with increasing precipitation depth becomes valid for more and more electrons. On the contrary, for the electrons precipitating within the loss cone per the second formula in equation (20), the converging magnetic field will decrease pitch angles, or increase μ in equation (19), but this becomes only effective at deeper atmospheric levels where the magnetic field reaches higher magnitudes.

Thus, at the depths above the transition region, 2×10^{19} cm^{-2}, where the self-induced electric field is rather strong (see Fig. 1) and magnetic field convergence is small or absent, the pitch-angle scattering in collisions is strongly affected by the self-induced electric field. Close to the injection point the electrons have $\mu \simeq 1$ and the effects of electric or magnetic fields are negligible. In spite of the electric field being strongest at the top, beam electrons still have enough energy and pitch angles small enough to precipitate to lower atmospheric depths. There are no electrons moving in the direction opposite to the beam, and the induced electric field is due solely to ambient electrons (Diakonov & Somov 1988).

With further precipitation, the electrons lose more and more of their energy due to collisions and the electric field and are also scattered to larger pitch angles. Some electrons eventually gain $\mu < 0$. These returning electrons now add to the self-induced electric field, and relatively fewer ambient electrons contribute to the return current as the depth increases. The returning electrons are also less scattered by collisions and they lose less energy to collisions since they are moving into lower density plasma. They are now accelerated by the electric field, since its direction coincides with the returning electron motion. This acceleration is larger for electrons, which turn around deeper in the atmosphere because they travel a larger distance in the same direction as the electric field.

If the electric field is not constant at all depths but decreases with depth from some turning point (see § 3.1), this can lead to the maxima at both energy (50–70 keV) and pitch angles $\sim\mu = -0.6$–0.7 in the electron distributions (see Figs. 3–7 in Zharkova & Gordovskyy 2005), which can be also confirmed by the extrema on E and μ in equations (18)–(19).

3.3.2. *Electron Distribution Functions*

Differential spectra.—The differential spectra calculated from the full kinetic equation (2) are plotted in Figure 8 for the beams with initial energy fluxes 10^8, 10^{10}, and 10^{12} ergs cm^{-2} s^{-1} and initial spectral indices of 3 and 7 (Zharkova & Gordovskyy 2005).

In the case of weak beams (10^8 ergs cm^{-2} s^{-1}; top plots in Fig. 8), when the induced electric field is weak and constant at most depths, the collisional depth (2×10^{19} cm^{-2} for $E_{\rm low}$) is shorter than the "electric" one (10^{20} cm^{-2}) found for the electric field from Figure 1. Thus, the beam precipitation is dominated by collisions and their resulting differential spectra toward lower energies become flatter with depth. This happens because the electrons that have higher energies at the start of precipitation shift to lower energies during their precipitation. However, their

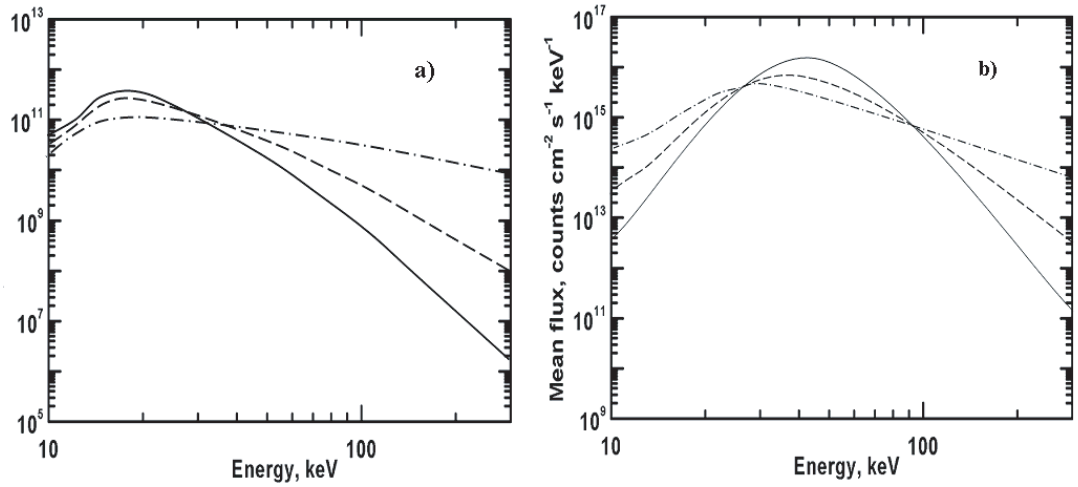

FIG. 9.—Mean electron spectra for a full kinetic solution (collisions + electric field) calculated for the initial fluxes 10^8 (*a*) and 10^{12} ergs cm^{-2} s^{-1} (*b*) and spectral indices $\gamma = 3$ (*dot-dashed lines*), 5 (*dashed lines*), and 7 (*solid lines*).

number was lower than the number of lower energy electrons because of the initial power-law energy distribution. Thus, with every precipitation depth a number of lower energy electrons will be constantly repopulated by a declining number of higher energy electrons. This leads to flattening of lower energy parts of the differential spectra (Syrovatskii & Shmeleva 1972) and at some chromospheric depths results in the appearance of the maxima in differential spectra at $E_{\max} = (\gamma + 1)E_{\rm low}$.

For stronger beams (10^{12} ergs cm^{-2} s^{-1}; bottom plots in Figs. 8*c* and 8*d*), their induced electric field is, first, substantially higher in the corona and, second, constant only at the depths about 10^{18} cm^{-2} (the turning point), after which it decreases either linearly (for harder beams) or parabolically or steeper (for softer ones). For higher electric fields the electric stopping depths move into upper atmospheric levels above the collisional one. For electrons with $E_{\rm low} = 12$ keV it moves to 4×10^{17} cm^{-2}, for 40 keV electrons to 2×10^{18} cm^{-2}, and only for 100 keV electrons to the depth lower than 2×10^{19} cm^{-2} that is the collisional stopping depth for $E_{\rm low} = 10$ keV.

The more intense and softer the beam is, the higher the magnitude of its constant electric field is (see § 3.2). Thus, the energy that electrons lose before the turning point is also higher and the differential spectra are flatter at lower energies. However, their turning point also shifts upward to the corona, which reduces the length of the constant electric field region and increases the depth range over which the self-induced electric field decreases. Hence, the energy losses of electrons between 10 and 100 keV are dominated by deceleration in the induced electric field.

Thus, electrons with energies 10–50 keV lose the bulk of their energy mostly in the constant electric field and only a little in collisions so that they all are turned into the returning electrons with the negative pitch angles as discussed in § 3.3.1. Electrons with initial higher energies 50–100 keV lose less of their energy in the electric field since it is decreasing with depth. At these depths they still do not lose enough energy in collisions because have not approached yet their collisional stopping depths. Then a lesser number of these electrons is turned to the negative pitch angles. As a result, the electron distributions have wide maxima at some intermediate energies 40–70 keV with the distributions becoming flatter toward both lower and higher energies.

For a given beam intensity, the softer the beam, the shorter the distance where the induced electric field is constant and the smaller is the energy lost by the electrons in this deceleration. As a result, the electrons with higher energy can reach deeper atmospheric depths between the turning point and the collisional stopping depth (compare the top and bottom plots in Fig. 8). In addition, harder beams induce an electric field that falls more smooth than the softer ones (see § 3.2). This also leads to a faster energy loss between the turning point and collisional stopping depth and to a narrower maximum in their differential spectra than for softer beams (compare Figs. 8*c* and 8*d*).

The positions of maxima in the differential spectra also depend on the beam parameters. For weaker beams, the maximum appears at lower energies and for stronger ones at higher energies (compare the bottom and top plots in Fig. 8). The maximum positions are defined by a bigger distance between the turning point and the collisional stopping depth (see § 3.2). The maxima are higher and wider for softer beams and lower and narrower for harder ones (compare the left and right plots in Fig. 8).

This can be explained by the fact that the more intense and softer the beams are, the shorter the constant part of the electric field is and the steeper its decrease is. The former means that the maximal energy of electron affected by the deceleration in the constant electric field is reduced (i.e., 60 keV for a beam of 10^{10} but only 30 keV for a beam of 10^{12} ergs cm^{-2} s^{-1}). The latter means that electrons with higher energies can precipitate in a decreasing electric field between to the depths, which are deeper than the electric stopping depth for the constant field but lower than their collisional stopping depth. This leads to a wider energy range in which electrons are "relieved" from the electric field—that is, in which they are less decelerated while still affected by collisions. This results in the maxima in differential spectra becoming wider and shifted to higher energies for softer intense beams (Fig. 8).

Pitch-angle distributions.—The pitch-angle distributions of precipitating electrons (with positive pitch angles) at any depth are just slightly wider than the initial normal ones assumed at the injection (see eq. [19] of this paper and Figs. 3–7 of Zharkova & Gordovskyy 2005). This happens because the distributions are formed from the initially higher energy electrons, which are scattered to smaller pitch angles, as discussed in § 3.3.1.

However, beyond some depth, a larger number of lower energy electrons have negative pitch angles (returning electrons) because of the pitch-angle changes in the electric field discussed in § 3.3.1. The distributions of returning electrons have maxima at $\mu \simeq -0.6$ to -0.8. For harder beams, the maxima appear at

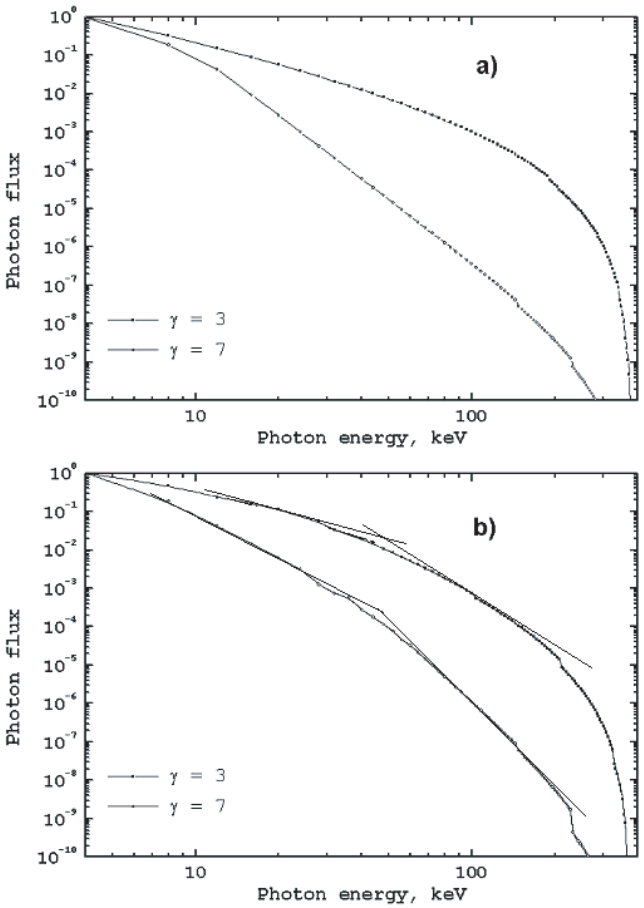

FIG. 10.—Photon spectra from the full kinetic solutions of beams with the initial energy flux of 10^8 (*a*) and 10^{12} ergs cm^{-2} s^{-1} (*b*).

lower energy and are narrower because of less electrons being affected by the electric field, and the opposite is true for softer ones, as discussed in § 3.2.

3.3.3. *Mean Electron Fluxes*

The full kinetic energy and pitch-angle distributions, discussed above, result in the mean electron spectra presented in Figure 9 for beams with $\gamma = 3$, 5, and 7 and with the initial energy flux of 10^8 (Fig. 9*a*) and 10^{12} ergs cm^{-2} s^{-1} (Fig. 9*b*).

Since for calculation of mean flux spectra we integrate the distribution functions over all pitch angles, the distributions of precipitating and returning electrons are added together. The maxima in the mean electron spectra appear at energies of 50–65 keV where there are maxima in the differential spectra in § 3.3.2 and in the pitch-angle distributions of returning electrons from § 3.3.2. The maxima in $\mathcal{F}$ shift toward lower energies and become narrower for harder beams as in the differential spectra. These maxima are likely to point out the electric field turning point followed by a decrease with depth of the electric field that is smoother for harder beams and steeper for softer ones as discussed in § 3.3.2.

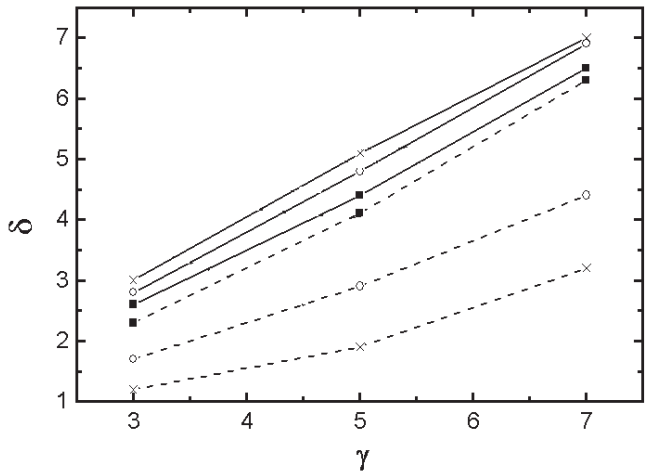

FIG. 11.—Photon spectral indices δ_{low} (*dashed lines*) and δ_{high} (*solid lines*) vs. electron indices γ for the initial energy flux of 10^8 (*squares*), 10^{10} (*circles*), and 10^{12} ergs cm^{-2} s^{-1} (*crosses*).

The mean flux spectra at lower energy parts are noticeably softer, or their indices are higher by about 0.8–1.2, for stronger beams than those for weaker ones (compare Figs. 9*a* and 9*b*), which indicates the domination of electric deceleration over collisions at higher precipitation depth. For stronger beams the mean flux indices after the maxima are also slightly softer than is expected from pure electric field solution, pointing to spectral softening in a variable electric field (see § 3.2.5).

3.3.4. *Photon Spectra*

The resulting photon fluxes (Fig. 10) calculated from the differential electron spectra above are "double power laws" (elbow-type), similar to the photon spectra deduced from the *RHESSI* observations (Holman et al. 2003). The photon spectral indices at lower energies, δ_{low}, and those at higher energies, δ_{high}, are presented in Table 2 for the accepted spectral indices and the initial energy fluxes of electron beams. It has to be noted that we assign a spectral index γ to the spectra of beam electrons and δ to their photon spectra that is different from the definitions by some other authors who used γ for defining the photon flux spectra (Brown 1971; Syrovatskii & Shmeleva 1972).

The photon indices δ_{low} and higher δ_{high} are found to be dependent on the beam initial flux and the electron beam spectral indices γ, as plotted in Figure 11. Note that δ_{high} slightly decreases with the initial energy flux and the electron spectral index γ (compare the solid curves with the crosses and dark squares). The spectral indices δ_{low} show a noticeable decrease compared to the electron indices γ for larger electron flux and, especially, with increased γ (compare the dashed curves in Fig. 11).

TABLE 2

PHOTON SPECTRAL INDICES δ_{LOW} AND δ_{HIGH} VS. SPECTRAL INDICES γ OF ELECTRON BEAM ENERGY SPECTRA

	FLUX = 10^8 ergs cm^{-2} s^{-1}		FLUX = 10^{10} ergs cm^{-2} s^{-1}		FLUX = 10^{12} ergs cm^{-2} s^{-1}	
γ	δ_{low}	δ_{high}	δ_{low}	δ_{high}	δ_{low}	δ_{high}
3.....	2.3	2.6	1.7	2.8	1.2	3.0
5.....	4.1	4.4	2.9	4.8	1.9	5.1
7.....	6.3	6.5	4.4	6.9	3.2	7.0

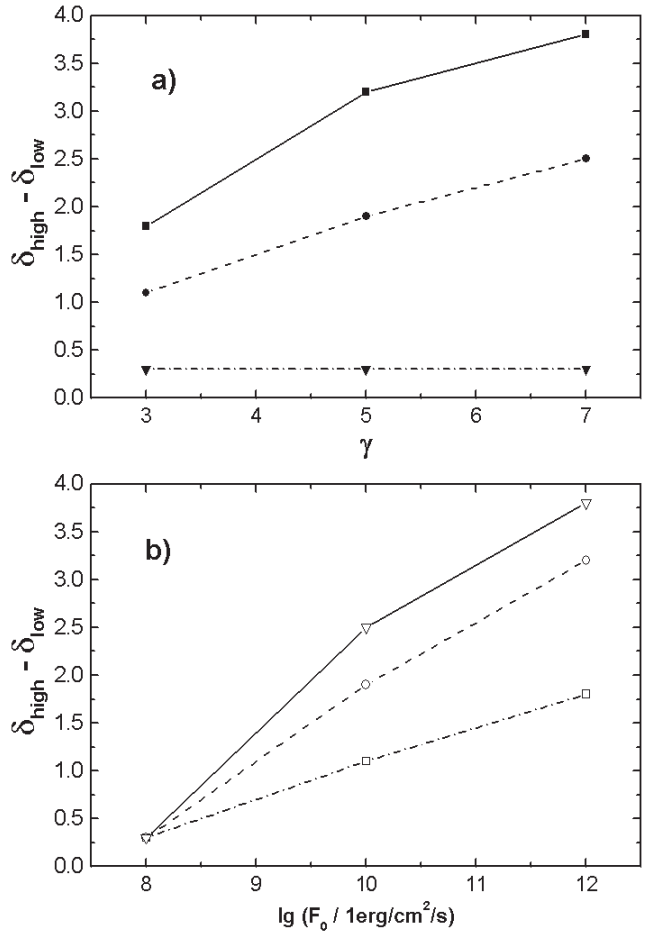

FIG. 12.—Photon spectral indices $\delta_{high} - \delta_{low}$ vs. electron spectral indices γ (*a*) and vs. the electron initial energy fluxes F_0 (*b*).

This is more apparent in the differences between the higher and lower energy photon indices, $\delta_{high} - \delta_{low}$, plotted in Figure 12 versus spectral indices γ and initial energy fluxes F_0. The differences grow significantly with increasing initial energy flux F_0 (Fig. 12*a*), i.e., with increasing absolute magnitude of the self-induced electric field. They also grow with increasing electron spectral index γ (Fig. 12*b*), i.e., as the turning point moves higher into the corona. The increase is more sensitive to the beam intensity, or to the magnitude of the induced electric field, than to the beam spectral index (compare Figs. 12*a* and 12*b*), showing some saturation for stronger and softer beams reported earlier by Emslie (1981).

These dependences can explain the spectral index variations during a single flare evolution, the "soft-hard-soft" patterns for the fluxes above 35 keV reported by many observers (e.g., see Fletcher & Hudson 2002; Grigis & Benz 2005), by injection of electrons beams with the same spectral index γ but with the "low-high-low" temporal profile of their energy fluxes. At the flare onset, the initial fluxes are smaller, as are the self-induced electric fields induced by the injected electrons. As a result, the photon spectra have indices close to δ_{high} without any flattening (soft spectra). At the flare maximum, the energy fluxes of electron beams are much stronger and induce much higher electric fields. This leads to a strong flattening of their photon spectra at lower energies with the index δ_{low} (hard spectra) because of the joint effect of collisions and electric field as discussed above. After the flare maxima the beam fluxes decrease again, which will result in smaller induced electric fields and the photon spectra with the indices δ_{high} (soft spectra) as at the flare onset.

4. CONCLUSIONS

We present analytical solutions for collisionless precipitation of power-law electron beams with the spectral index γ in a presence of electric field and compare these solutions with full kinetics ones obtained numerically from the Fokker-Planck-Landau equation for the beams with the initial energy fluxes of 10^8 and 10^{12} ergs cm^{-2} s^{-1} and the initial spectral indices of 3, 5, and 7.

The differential spectra of beam electrons injected with power-law energy spectra are found analytically from the continuity equation in a pure electric approach for a constant and variable electric field. The precipitating electron with energy E is shown to steadily lose the same amount $e\mathcal{E}x$ of their energy with a precipitating distance x in a flaring atmosphere until they are fully decelerated by the constant electric field $\mathcal{E}$ at the "electric" stopping depth $x_{\mathcal{E}} = E/eE$. The returning electrons are found to be linearly accelerated to energies proportional to the electric field magnitudes and the distances at which the particle started its acceleration, or turned to the pitch angles larger than $\pi/2$.

Deceleration of precipitating beam by a constant electric field is found to affect mainly the lower energy electrons (<100 keV) by significantly reducing their number at the upper precipitation depths in the corona. This leads to flattening toward the lower energies of their differential spectra. This results in the mean electron flux having the spectral index $\beta_E = \gamma - 1$ and the photon spectra having the index $\delta = \gamma$. For the electric field decreasing with depth, the deceleration by electric field also decreases that leads to less energy losses and less flat differential spectra. The mean fluxes produced by the electrons in a variable field falling with depth as $1/x^k$ have the spectral indices $\delta \simeq \gamma + k/(k+1)$.

The combined electric field, with a constant part in the corona and a variable part in deeper layers, reveals fast flattening of the differential spectra and mean electron fluxes at lower energies, similar to those for the constant field, with much smaller flattening for intermediate energies (50–100 keV), where the electric field is decreasing with depth (variable field) and softening for higher energies.

A joint effect of the electric field and collisions considered in the full kinetic approach results in the maxima in electron differential spectra appearing owing to a deceleration in the induced electric field at higher energies compared to pure collisions. The self-induced electric field found from the full kinetic simulations reveals a constant part in the upper corona and a steeply decreasing part in deeper atmospheric layers. The magnitudes of a constant part and the steepness of a decreasing part strongly increases with increasing electron spectral indices and energy fluxes.

Because of the induced electric field profile, the electrons with energies 10–50 keV lose their energy mostly in a constant electric field and slightly in collisions. The electrons with higher energy (50–100 keV) are less decelerated by a decreasing electric field and still do not lose much energy in collisions, because they do not reach yet the collisional stopping depth for the electrons with a lower cutoff energy.

This results in flatter differential distributions toward lower energies, which appears much higher in the corona (closer to the injection site) compared to pure collisions. Because of collisional losses the differential spectra at higher energies show a decrease again leading to the maxima. The more intense the electron beam is, the higher the magnitude is of a constant electric field and, thus, the energy of the maxima. On the other hand, the softer the beam, the shorter the distance where the induced electric field is constant, and the smaller the energy lost by the electrons in this deceleration.

As a result, the electrons with a wider energy range can reach the depths between turning point and the collisional stopping depth. This leads to faster losses of electron energies between the turning point and the collisional stopping depth and to the narrower maxima in their differential spectra, than for softer beams. It has to be noted that the differential spectra are formed by both precipitating ($\mu > 0$) and returning ($\mu < 0$) electrons since they are integrated over pitch angles. In the distributions lower energy electrons are mostly the electrons back-scattered to larger pitch angles above $\pi/2$, and at very early precipitation depths they replace the ambient plasma electrons in the return current.

The maximum energy in the mean fluxes found from the simulations is slightly dependent on the beam spectral index and initial energy flux. For very intense beams the maximum energy changes from 40 keV for $\gamma = 3$ to 60–65 keV for $\gamma = 7$, and for weaker beams it noticeably decreases. These maxima in the mean electron spectra combined with the thermal spectra can lead to the dips at lower energies of about 10 keV deduced in mean electron fluxes from the *RHESSI* observations (Brown et al. 2003). Apparently, the energy of these maxima defines the energy (and depth) of the induced electric fields between the turning points and the collisional stopping depths.

The differential spectral flattening leads to double power-law photon spectra similar to those reported from the *RHESSI* observations (Holman et al. 2003). However, these photon spectra are produced by beam electrons with the same spectral index γ with the flattening at lower energies owing to energy losses in a self-induced electric field. The differences between the lower and higher spectral indices in the resulting photon spectra and the break energy separating the lower and higher energy elbows increase with increasing initial energy fluxes and spectral indices of the injected electrons.

This joint effect of collisions and Ohmic losses on photon spectra can explain the well established "soft-hard-soft" pattern in the photon spectral indices during the evolution of a single solar flare by an electron beam with the same spectral index having the low-high-low profile for its initial energy flux, or the induced electric field.

The authors would like to express their deepest gratitude to Professor John Brown of Glasgow University, UK, for his very valuable comments and general discussion of the paper during its preparation from which the paper strongly benefited. We appreciate the constructive comments by our anonymous referee that helped to make the paper more lucid. The authors also acknowledge the contribution of Professor A. G. Emslie of Oklahoma University, US, and Professor John Brown of Glasgow University to the general discussion of the problem of a return current at the *RHESSI* Workshop in Sonoma, California, where the main ideas of the paper were formulated. We also very much appreciate the discussion with John Baruch of Bradford University that improved our paper presentation.

REFERENCES

Benz, A. O. 2002, Plasma Astrophysics: Kinetic Processes in Solar and Stellar Coronae (2nd ed.; Dordrecht: Kluwer)
Brown, J. C. 1971, Sol. Phys., 18, 489
Brown, J. C., Emslie, A. G., & Kontar, E. P. 2003, ApJ, 595, L115
Brown, J. C., Spicer, D. S., & Melrose, B. D. 1979, ApJ, 228, 592
Conway, A. J., Brown, J. C., Eves, B. A. C., & Kontar, E. 2003, A&A, 407, 725
Diakonov, D. V., & Somov, B. V. 1988, Sol. Phys., 116, 119
Emslie, A. G. 1980, ApJ, 235, 1055
———. 1981, ApJ, 249, 817
Fisher, G. H., Canfield, R. C., & McClymont, A. N. 1984, ApJ, 281, L79
Fletcher, L., & Hudson, H. S. 2002, Sol. Phys., 210, 307
Gordovskyy, M., & Zharkova, V. V. 2003, in Proc. PREP-2003 Conference on Electronics, Software and Communications, Vol. 2 (Exeter: Exeter Univ. Press), 187
Grigis, P. C., & Benz, A. O. 2005, A&A, 434, 1173
Haug, E. 1997, A&A, 326, 417
Haydock, E. R., Brown, J. C., Conway, A. J., & Emslie, A. G. 2001, Sol. Phys., 203, 355
Holman, G. D. 2003, ApJ, 586, 606
Holman, G. D., Sui, L., Schwartz, R. A., & Emslie, A. G. 2003, ApJ, 595, L97
Knight, J. W., & Sturrock, P. A. 1977, ApJ, 218, 306
Kontar, E. P., Brown, J. C., Emslie, A. G., Schwartz, R. A., Smith, D. M., & Alexander, R. C. 2003, ApJ, 595, L123
Kontar, E. P., Brown, J. C., & McArthur, G. K. 2002, Sol. Phys., 210, 419
Lang, K. R. 1974, Astropysical Formulae, Vol. 1 (Berlin: Springer), 93
Lin, R., et al. 2003, ApJ, 595, L69
Massone, A. M., Emslie, A. G., Kontar, E. P., Piana, M., Prato, M., & Brown, J. C. 2004, ApJ, 613, 1233
McClements, K. G. 1992, A&A, 258, 542
Nagai, F., & Emslie, A. G. 1984, ApJ, 279, 896
Piana, M., Massone, A. M., Kontar, E. P., Emslie, A. G., Brown, J. C., & Schwartz, R. A. 2003, ApJ, 595, L127
Somov, B. V., Sermulina, B. J., & Spektor, A. R. 1982, Sol. Phys., 81, 281
Somov, B. V., Spektor, A. R., & Syrovatskii, S. I. 1981, Sol. Phys., 73, 145
Syrovatskii, S. I., & Shmeleva, O. P. 1972, Astron. Zh., 49, 334
Zharkova, V. V., Brown, J. C., & Syniavskii, D. V. 1995, A&A, 304, 284
Zharkova, V. V., & Gordovskyy, M. 2005, A&A, 432, 1033
Zharkova, V. V., & Kobylinskii, V. A. 1993, Sol. Phys., 143, 259